# Analysing the impact of compaction of soil aggregates using X-ray microtomography and water flow simulations

*Menon M[1], Jia, X[2], Lair GJ[3,4], Faraj, PH[1], Blaud A[1]

1. Department of Civil and Structural Engineering, Kroto Research Institute, University of Sheffield, Broad lane, Sheffield S10 5SX

2. Department of Particle Science and Engineering, University of Leeds, LS2 9JT

3. University of Natural Resources and Life Sciences (BOKU), Vienna, Peter-Jordan-Str. 82, 1190 Vienna, Austria

4. University of Innsbruck, Institute of Ecology, Sternwartestr. 15, 6020 Innsbruck, Austria.

*corresponding author
Department of Civil and Structural Engineering, Kroto Research Institute,
University of Sheffield, Broad lane,
Sheffield S10 5SX,
United Kingdom.
E-mail: m.menon@sheffield.ac.uk
Tel: +44 (0) 114 222 5752

***Keywords:*** *soil compaction, soil aggregates, X-ray microtomography, Lattice Boltzmann, modelling, water flow*

## Abstract

Soil aggregates are structural units of soil, which create complex pore systems controlling gas and water storage and fluxes in soil. Aggregates can be destroyed during swelling and shrinking or by external forces like mechanical compaction and yet, the knowledge of how physical impact alters aggregate structure remains limited. The aim of the study was to quantify the impact of compaction on macroaggregates, mainly on the pore size distribution and water flow. In this study, aggregates (2 - 5 mm) were collected by dry sieving in grassland of the Fuchsenbigl-Marchfeld Critical Zone Observatory (Austria). The structural alterations of these soil aggregates under controlled compaction were investigated with a non-invasive 3D X-ray microtomography (XMT). The detailed changes in pore size distribution between aggregates (interpores, diameter >90 μm) and within the aggregates (intrapores, diameter ≤90 μm) in pre-and post-compacted soils were revealed at two soil moisture (9.3% and 18.3% w/w) and two compaction increments (0.28 and 0.71 g $cm^{-3}$ from the initial values). The soil permeability was simulated using lattice Boltzmann method (LBM) based on 3D images. Soil compaction significantly reduced total pores volume and the proportion of interpores volume and surface area, while total pore surface area and the proportion of intrapores volume and surface area increased. The increases in soil moisture tended to reduce the effects of compaction on interpores and intrapores, while the high compaction increment drastically changed the pore size distribution. The aggregate compaction decreased water penetration potential due to the increase of small intra-aggregate pores and cavities as demonstrated by LBM. Notably, the model results showed that a significant linear correlation between the water flow rate and bulk density of soil aggregates, predicted the risk of complete stoppage of water flow at bulk density of ≥ 1.6 g $cm^{-3}$ at a soil water content of 18 % w/w. Thus, a combination of imaging and modelling provided new insights on the compaction effects on aggregates, underpinning the importance of protecting soil structure from mechanical compaction to minimise environmental impacts of soil compaction and maintain water infiltration and percolation in arable soils.

## 1. Introduction

Aggregates are the structural units of soils with different size and shape, and are formed by the agglomeration of mineral particles (i.e. clay, silt and sand) and a variety of binding agents such as roots, fungal hyphae and microbial polysaccharides, calcium bridges and different (hydr)oxides (Six et al., 2004; Tisdall and Oades, 1982). The structure and stability of aggregates is crucial for water infiltration and movement, gas exchange, soil erosion, biological activity and rooting influencing the growth of crops (Hillel, 1998; Amézketa, 1999; Bronick and Lal, 2005).

Soil compaction is the densification of soil by application of mechanical energy (Holtz 2010), which can occur naturally or driven by anthropogenic activities. The result is an increase of bulk density and a reduction of pore space, affecting the percolation of soil water as well as gas exchange or production. Soil compaction has been strongly linked to the loss of nitrogen by the accelerated production of greenhouse gases (e.g. $N_2O$) through denitrification in anaerobic conditions (Keller et al., 2013).

Due to above ecological impacts, soil compaction has been widely recognized as a soil threat by many regional, national and international organisations (Hartemink, 2008; Banwart, 2011). It has been described as an 'unnecessary form of land degradation' by Food and Agricultural Organization (FAO, n.d). In Europe, compaction is widespread and it accounts for about 17% of the total area of degraded soil (EEA, 2012). The EU Soil Thematic Strategy identified compaction as one of the major soil threats in Europe (COM, 2006).

Most of the studies investigating soil compaction were conducted using bulk soils under lab or field conditions. However, the compaction of soil aggregates was rarely investigated despite the fact that the size distribution of aggregates has been often used as an indicator of soil fertility. For example, an empirical rule suggests that a soil structure consisting of more than 60% of macro-aggregates (0.25-10 mm) can be classified as "agronomically valuable" (Shein, 2005). The size and stability of soil aggregates regulate gas and liquid diffusion in soil (Sexstone et al., 1985; Horn and Smucker, 2005), enhance the accumulation of soil organic matter by physical protection (Bossuyt et al., 2002), provide specific microbial habitats and directly influence microbial composition and activity (Blaud et al., 2012). However, soil aggregates turnover (i.e. cycles of formation and natural disruption of aggregates) (Stamati et al.,

2013) is easily disturbed in presence of external factors such as tillage or compaction. In particular macroaggregates (diameter >0.25 mm) are disrupted the most. However, there is a limited mechanistic understanding how breakdown of macroaggregates occur and how this can affect the movement of air and water in soils.

Dexter (1988) proposed three main changes in soil aggregate structure during compaction depending on soil moisture content. Firstly, when soil aggregates are dry and hard, the soil particles will be rearranged under compaction. Secondly, when aggregates are weak or brittle, fracture will occur and broken aggregate fragments may fill up the spaces between existing soil aggregates and particles. Thirdly, aggregates are plastic and when compacted, the compression creates plastic flow with flat areas of contact between the aggregates. However, the dynamics of pore space in these scenarios are to be studied in order to produce meaningful predictions on water or air flow; i.e., further insights are needed on how compaction affect the internal (intra-aggregate pores or intrapores) along with changes in porosity between them (inter-aggregate pores or interpores) as well as overall pore size distribution.

Compaction is a multidisciplinary problem and several methods can be used to study structural alterations in soils. Thus, a selection of method for studying compaction will depend on the research context and resources available (see review from Keller et al., 2013). Total porosity can be calculated by measuring bulk density and the soil density in laboratory. Odometer is also used widely to study compaction. However, these methods do not provide information about pore size distribution in the sample and for this, the soil water retention curve has to be measured using the pressure plate apparatus. Imaging tools can yield high resolution 2D or 3D images of pore space. For 2D imaging, thin sections are made from resin impregnated soil samples and images are processed for different pore characteristics (Murphy, 1986). This method suffers from the problem of destructive sampling, and cross sections do not provide information on the real 3D geometry of the pores in samples. In contrast, using the advanced 3D imaging tools such as XMT (X-ray microtomography, also known as micro-CT) and image analysis software, it is now possible to study the pore size characteristics with very high spatial resolution (up to a few microns, depending on the sample size) non-destructively (Mooney et al., 2012). In addition, the data from XMT can be directly used for modelling to quantify processes such as diffusion of fluids. However, imaging methods suffers from the fact that the resolution depends on the sample diameter.

Despite its several advantages, it has not been used widely to study soil compaction. Few studies have already demonstrated the water flow through aggregates using 2D images (Aravena et al., 2014; Berli et al., 2008; Carminati et al., 2007). Notably, Aravena et al. (2014) showed that localized compaction of aggregates at the rhizosphere increased the flow of water towards the root by 27%. An alternative modelling method is available, that uses 3D image data is Lattice Boltzmann Method (LBM), which is simpler and faster and do not require finite element meshing of images as demonstrated earlier by Menon et al. (2011).

The aim of this laboratory study was to investigate the impact of compaction on a pack of soil aggregates on its pore structure and water flow with the following specific objectives: 1) visualize and quantify inter- and intra-aggregate pores in compacted soils, 2) compare the effect of soil moisture content and different compaction strengths on the pore size characteristics (inter and intra aggregate porosities and pore volume distribution) of soil aggregates, 3) predict the effect of compaction on water flow using LBM.

## 2. Materials and Methods

### *2.1. Soil sampling and preparations*

Dry sieved soil aggregates were collected from bulk soil below the main rooting zone (5-10 cm soil depth) at an agriculturally used grassland site located in Fuchenbigl-Marchfeld Critical Zone Observatory in September 2011. The field site is located east of Vienna, Austria, in the National Park "Donau-Auen" and developed on approx. 350 year old alluvial Danube River sediments (48°11'N, 16°44'E; Lair et al., 2009). The soil aggregate distribution of bulk soil (5-10 cm soil depth) obtained by wet sieving (Haynes and Swift,1990) revealed the following aggregate size distribution: <0.25 mm (6.1%), 0.25-0.5 mm (6.9%), 0.5-1 mm (5.2%), 1.0-2.0 mm (14.5 %), 2.0-5.0 mm (37.8%) and 5-10 mm (21.5%). More than 90% of the aggregates were water stable. Therefore, the predominant aggregate size class of 2-5 mm was selected for this study. Particle size distribution in this aggregate size class was 78 g $kg^{-1}$ sand, 644 g $kg^{-1}$ silt and 278 g $kg^{-1}$ clay. The organic C concentration was 49.0 g $kg^{-1}$ and total N 33.8 g $kg^{-1}$in the studied aggregates.

To study the effect of soil compaction, samples were prepared with two different moisture levels: 1) aggregates with gravimetric water content of 9.3% (W1), representing the field moisture content at the time of sampling, and 2) an elevated moisture content of 18.3% (W2), at which aggregates were only slightly plastic and thus easier to handle in imaging experiments. For the latter, the aggregates were saturated with water first and air-dried until the desired soil moisture was attained. Soil aggregates were weighed and filled into a specially designed plastic cylinder (14.9 mm inner Ø and 60 mm height) with a piston. The size of the plastic cylinder was particularly selected in order to fit (sample size limits for the imaging device: 60 mm length and 50 mm diameter) the imaging device as well as to achieve a resolution of 10 µm. The bottom of the container was sealed with a flat metal sheet. Three replicated samples were used for the two moisture and compaction levels, respectively, using the same weight (4.14 g for W1 and 4.84 for W2) of aggregates. Soil aggregates were filled and gently tapped to settle the aggregates in the cylinder and the initial bulk density was calculated using the mass-volume relationship. All samples were imaged before compaction to get initial pore structure (details on imaging is provided in the following section) and then compacted by pushing the soil by hand with the help of small piston (custom made to fit the cylinder) with occasional pounding to achieve the required bulk density increment of 0.28 (BD1) and 0.71 g $cm^{-3}$ (BD2). Due to the multiple impacts involved, we could not precisely measure the load applied on the samples. In order to measure the maximal approximate load applied, a separate uniaxial load testing was carried out using a mechanical tester (Instron, model: 5566). Maximal loads required to reach W1BD1 and W2BD1 were 185 (±1.8) kPa and 116 (±2.6) kPa, respectively, and for W2BD2 it was 530 (±11) kPa.

The high compaction level (BD2) was only performed on samples with gravimetric water content 18.3% (W2), because they were more compressible than the ones at lower soil water content (W1). Samples were imaged again after applying compaction. Table 1 shows the treatment combinations, bulk densities and the maximal load applied.

*2.2. Imaging and Image Processing*

X-ray microtomography (XMT) has become a popular tool to characterize soil structure in recent years. The method has been previously used to study pore structure under mechanical disturbance of fragile biological crusts (Menon et al., 2011) and a similar methodology was followed in this study. Pre and post-compacted samples were imaged using XMT at 10 µm resolution (Model: Skyscan 1172 with a detector array of 2000 x 1048 pixels) available at the University of Sheffield. Images were reconstructed and processed with Simpleware (v6) with a final effective pixel resolution of 30 µm to fit the capacity of the desktop system (16GB RAM with i7 quad core processor).

The pores were divided into two main groups based on their size and location: 1) inter-aggregate or interpores, which are the pores between soil aggregates, 2) intra-aggregate pores or intrapores within soil aggregates (pores within the solid matrix of soil aggregates which are mostly <90 µm in size). This size was selected based on several preliminary image analyses of the data from the pre-compacted samples. It should be noted that intrapores also include a small fraction of pores between contact surfaces of aggregates but they are impossible to exclude in 3D volume image processing.

In order to separate inter- and intrapores, the following simple steps as shown in Figure 1 were followed. First step of image processing is the *segmentation* of images using an appropriate pixel threshold to separate solids and pores. A *floodfill* operation (i.e. it joins the regions with similar pixel values) was then carried out. A *median filter (2 pixels)* was then applied to remove the noise in the image, resulting a 'soil mask'. To separate the intrapores a *morphological close* filter (3 pixels, 90 µm) was applied to produce 'soil solid mask' (i.e. closure of all intrapores) and intrapores can then be quantified by Boolean image subtraction operation (i.e. intrapores = soil solid mask - soil mask). A separate cylinder mask was then created to represent the sample volume in order to quantify the interpores, for which the Boolean subtraction operation was used again (i.e. interpores = cylinder mask - soil solid mask).

Although the entire length of most cylinders were scanned, it was computationally challenging to process entire length (unable to upload full dataset on Simpleware) and therefore top 1 cm and bottom 0.8 cm (the length of W2BD2 treatment after compaction was 1.8 cm and hence was used for all samples for uniformity) of each sample were used for further processing. However, after the image analysis of both parts of the columns separately, it was found that the inter- and intrapores volume and surface was not significantly different between the top and bottom part of the samples. Thus, the average of the top and bottom were used for the figures presented in this study and for statistical analysis.

The outputs of the analysis gave the total volume ($mm^3$) and total surface area ($mm^2$) for inter- and intrapores which were also expressed as the proportion of the total pore volumes or surface area per sample in the paper. This was done because of the change in total volume of samples after compaction (Table 1). Furthermore, from these images, it was possible to quantify individual pore volumes and to present the pore volume distributions before and after soil compaction. However, it was only possible to count individual interpores and its volume; the software could not handle these tasks for intrapores. This is presumably due to the large number of intrapores created in compacted soils compared to interpores.

### *2.3. Modelling Flow using Lattice Boltzmann Method (LBM)*

More details on this method can be found in earlier publication (Menon et al., 2011), only a brief account of relevant aspects of the LBM model (code: D3Q19) is given here. It is highly effective in trend analysis and compared with conventional computational fluid dynamics (CFD) models, LBM is simpler and faster when used to calculate flow through a complex network of pores obtained from 3D images. Its simplicity is partly due to its formulation which is based on a regular (Cartesian) lattice grid – the same type employed in 3D imaging. Its speed is largely also due to the same reason, since no meshing or re-meshing step is required (which could take much longer than the actual flow calculations). Typically, through rescaling in the model formulation, LBM input and output are expressed in lattice units. For example, length is specified in *lu* (length unit), time in *ts* (time step), velocity in $lu\ ts^{-1}$, and kinematic viscosity in $lu^2\ ts^{-1}$. Nominally, both *lu* and *ts* are set to 1 to simplify calculations. LBM simulations are usually performed in a setup that helps to ensure numerical stability, then the results are rescaled to match the required, for instance, superficial velocity by taking advantage of the laws of similarity in fluid mechanics. LBM is known to be applicable only in low Mach numbers. It is assumed that flow pattern remains the same within a certain range of Reynolds number (e.g. creeping flow regime). To convert between lattice units and physical units, it is usually assumed that dimensionless ratios such as

Reynolds number or drag force coefficient are equal across the different (LBM and physical) systems. Take superficial velocity as an example, if Re (= $UL/v$) is assumed to be equal, the following equation can be used to convert LBM calculated velocity in lattice units to real velocity in physical units:

$$\mathrm{U}_{\mathrm{phys}} = \frac{\nu_{\mathrm{phys}}}{\mathrm{L}_{\mathrm{phys}}}\mathrm{Re}_{\mathrm{lattice}} = \frac{\nu_{\mathrm{phys}}}{\mathrm{L}_{\mathrm{phys}}}\frac{\mathrm{U}_{\mathrm{lattice}}\mathrm{L}_{\mathrm{lattice}}}{\nu_{\mathrm{lattice}}} \tag{1}$$

where $L$ is a characteristic length, $\tau$ a relaxation parameter in LBM and is related to kinematic viscosity by $v = (2\tau\text{-}1)/6$. In practice, $\tau$ is typically set to 1 and was the case in those current simulations. The driving force for flow in our LBM implementation is a user-definable, constant body force, $f_b$. Its value is typically set to a value below 0.015 for the sake of numerical stability. In our simulations it was set to 0.001. A constant body force is equivalent to a constant pressure gradient throughout the domain. Fluid density is customarily set to a nominal value of 1. During a LBM simulation, calculated superficial velocity is monitored and the simulation was stopped once this value became stable over a few hundred steps.

The final superficial velocity in physical units is equivalent to Darcy hydraulic conductivity. Permeability, as defined in Darcy law, is calculated using LBM input (ρ, $v$ and $f_b$) and output ($U$) as

$$K = \frac{U\rho v}{f_b} \tag{2}$$

It has the units of $lu^2$.

The LBM simulations were carried out only for elevated moisture level (18.3%) treatment because three bulk density levels were available (0.9, 1.2 and 1.6 g $cm^{-3}$). Due to small sample size and nature of this study (e.g. samples were imaged in pre and post-compacted condition), it was nearly impossible to measure the hydraulic conductivity in order to compare the results from modelling.

*2.4. Statistics*

The effect of soil compaction on soil pores (total pores, interpores and intrapores) volume and surface area was investigated using paired Student's t-Test (as the porosity of the same samples was measured before and after soil compaction). The effects of soil moisture level and compaction level were investigated using unpaired

Student's T-test. All the statistical analyses were performed using R version 3.1.0 (R Development Core Team, 2013).

## 3. Results

### *3.1. Visualization of Pore Characteristics*

Reconstructed images from XMT were processed using 3D imaging tools to visualize and quantify pore characteristics following the protocol described earlier (Fig. 1). Figure 2 shows a comparison of aggregates (top 1 cm) before and after compaction in 3D with respect to its changes in solid phase and pore space (inter- and intrapores) of the same sample W2BD2 (see Table 1) where the most impact on soil porosity was observed. As a result of compaction, the identities of individual aggregates were almost lost and all aggregates seemed to join together to form a single solid mass (see Fig. 2a and 2b). From these images, it can be directly seen that interpores were strongly reduced (both number and the amount; see Fig. 2c and 2d) and a sharp increase in number of intrapores (defined here as <90 μm sized pores) in compacted soils was found (detailed quantified data shown in section 3.2 - 3.4; see Fig. 2e and 2f).

### *3.2 Effect of soil compaction on total porosity*

Using 3D image processing tools, the total pore volume in all samples was calculated with an average of 741 ± 90 $mm^3$ ($n$ = 18) before compaction and the total pores surface area was on average 6875 ± 2471 $mm^2$ ($n$ =18) as shown in Figure 3. Soil compaction significantly ($P$ < 0.001) decreased the total pore volume by ~35% for a net change in bulk density of 0.28 g $cm^{-3}$ (BD1) regardless the soil moisture. Similarly, the effect of added moisture with higher compaction level (W2BD2) also produced significant reduction in the volume of pores by 66% (Fig. 3a). In contrast, the total pore surface area significantly ($P$ < 0.01) increased with soil compaction, by ~25% with an increase in bulk density of 0.28 g $cm^{-3}$ (Fig. 3b) and by 37% with an increase in bulk density of 0.71 g $cm^{-3}$ but the difference was not significant ($P$ = 0.1). Similar trend was also found for W2BD2 treatment; though there was an increase in pore surface area, it was not statistically significant.

*3.3. Effect of soil compaction on inter and intrapore size characteristics*

In this section, the impact of compaction on interpores and intrapores is presented in two ways; *first*, by the proportion of inter and intrapores (Fig. 4) and *second*, by their actual volumes (supplementary material, Fig. S1). Interpores dominated the total pores volume in comparison to the intrapores, representing >90% of the total pore volume before compaction in pre-compacted samples, however, after compaction there was an increase in intrapores in all cases (Fig. 4 a, b). The increase in gravimetric soil water content from 9.3% to 18.3% (w/w) significantly ($P < 0.001$) decreased the proportion of interpores volume by 22% (W1BD1) and 7% (W2BD1) and in the case of W2BD2 the decrease was 59% (Fig. 4a). In all cases, the decrease in interpores produced a corresponding increase in intrapores (Fig. 4b).

In the case of surfaces area of inter and intrapores, similar shifts were observed. The proportion of surface area of interpores decreased by approximately 18% in both compaction intensities (i.e. W1BD1 and W2BD1). However, for the treatment with higher water content with higher compaction intensity (W2BD2), the reduction was 39% (Fig. 4c), with a corresponding increase in surface area of intrapores (Fig. 4d). Thus, the effect of compaction on surface area of inter and intrapores was significant ($P < 0.001$).

These trends are further illustrated in Figure S1 in their actual values. The interpores volumes decreased by 53% at soil water content 9.3% but by 39% with higher soil water content under same compaction intensity (W1BD1 and W2BD1) and by 88% in high moisture and high compaction treatment (W2BD2) (Fig. S1a). In the case of intrapores, their volumes increased significantly ($P < 0.05$) by 53% (W1BD1), 58% (W2BD1) and 73% (W2BD2) (Fig. S1b). At higher soil water content, soil compaction did not significantly ($P = 0.77$) affect the interpores surface area, while it was reduced by 20% at low soil water content (Fig. S1c). Strikingly, only high level of soil compaction decreased (by 60%) the interpores surface area while no change was found a low level of compaction (BD1). In contrast, intrapores surface area increased by 44% for W1BD1, 52% for W2BD1 and 66% for W2BD2.

*3.4. Size distribution of interpores*

Figure 5 shows the changes in the interpore volumes (i.e. volume of individual interpores) before and after compaction along with the changes in the interpores numbers for one replicate. The trends were similar for the different replicates (data not shown). The increase in soil moisture resulted in a higher number of interpores with a volume <0.0001 $mm^3$ (Fig. 5b), in comparison to the low soil moisture samples (Fig. 5a). It is clear from these figures that soil compaction increased the total number of interpores due to the increase in the number of small interpores (<0.001 $mm^3$), although the total volume of interpores decreased sharply. The number of interpores was on average ($n$ = 3), for W1BD1 samples increased from 260±150 before compaction to 695±53 after compaction. For W2 BD1, this change was 59±32 before compaction and 838±60 after compaction whereas for W2 BD2, the number of pores increased from 120±21 before compaction to 670±45, after compaction. In contrast, the interpores volume was on average ($n$ = 3) for W1 BD1 samples 1338±323 $mm^3$ before compaction and 279±18 $mm^3$ after compaction, for enhanced soil water content (W2BD1) 2460±1941 $mm^3$ before compaction and 494±23 $mm^3$ after compaction, and for high compaction level (W2 BD2) 1465±163 $mm^3$ before compaction and 73±31 $mm^3$ after compaction. The interpores volume was dominated by a single interpore volume (0.0001 $mm^3$) before and after compaction, and representing >99% of the total volume for W1 BD1 and W2 BD1 (Fig. 5, and see Fig. 2c for images). It was only at higher level of soil compaction (W2 BD2), that the proportion of this large interpores was reduced to 70% on average (Fig. 5c).

### *3.5. Simulations of water flow*

The LBM simulations were carried out to compare two compaction levels for elevated moisture levels to predict how pore structure influences the water flow. The LBM provides both visualization as well as quantification of the flow through the porous medium. Thus, Figure 6a shows a cross sectional view of flow rate distribution, simulated by LBM, from the top part of one of the replicates with gravimetric water content 18.3% and bulk density before and after compaction 0.92 and 1. 67 g $cm^{-3}$. The images clearly show there was more velocity channels occurring in uncompacted soil samples than after compaction, where the pores were smaller and disconnected from each other.

The relationship between the simulated real velocity obtained by LBM and bulk density of all the samples was a negative linear correlation ($R^2$ = 0.96). An increase in bulk density of only 0.3 g $cm^{-3}$ (i.e. from 0.9 to 1.2 g $cm^{-3}$) decreased by 25% the real velocity. However, an increase in bulk density by 0.7 g $cm^{-3}$ (from 0.92 to 1.62 g $cm^{-3}$) nearly stopped the water flow (Fig. 6b).

## 4. Discussion

### *4.1 Shifts in interpores - intrapores balance in compacted soils*

The data clearly show significant reduction in total pore volume before and after compaction in all treatments with an increase in total pore surface area. However, this data do not provide enough insights into shifts in interpore and intrapore balance in compacted soils. The distinction of interpores and intrapores was found useful to gather better insights into the effect of soil compaction on soil porosity. It was for the first time, such analysis was carried out and the increase of intrapores after compaction was rather surprizing. Though intrapores only represent a small fraction of the total pore volume, it is often ignored because it cannot be measured easily. However this work has shown that there is a balance between inter and intrapores in a unit volume of soil and this balance is affected by compaction.

The simple method used in segmenting the 3D images to calculate inter and intrapores have been found very useful to understand changes in soil porosity caused by compaction. Intrapores include all pores within aggregates including cavities or “closed” pores. In some cases, large intrapores (>90 µm; Menon, pers. comm., 2014) are found in aggregates; however such cases were not found in our study. The intrapore size threshold (<90 µm) used in this study is very specific and it may vary according to the sample type. It must be also noted that pores are highly irregular in their shapes and sizes and in particular, when aggregates are loosely packed (i.e. before compaction), a few large interpores occupy significant proportion of the pore volume. Hydraulically, this is better for drainage of soil compared to a large number of fragmented pores after compaction.

Our data showed that when soil was compacted, intrapores volume and surface areas increased significantly after compaction (Fig. 4) at the expense of interpores; at the same time the number of interpores increased significantly along with its size distribution (Fig. 5). These changes can be explained in 3 ways. As a first stage of compaction, soil aggregates rearrange, which leads to a reduction of interpore volume. Such a rearrangement occurs only if the strength of the aggregates (depending on soil moisture content) is high enough to resist the load. This may not always involve deformation of soil aggregates. Next stage may include rupture of aggregates, followed by a flow of broken materials into the interpore space (Dexter, 1988) and this may occur when aggregates are dry and brittle as in the case of W1BD1 treatment (see Fig. 3). Soil moisture content will play significant part in this process (explained in the next section). However, when the soil aggregates are sufficiently plastic under elevated moisture content with sufficient loading (W2BD2), we can expect a plastic flow of materials into interpore space. Finally, with further application of load, interpores will gradually disappear. This will result in consolidated 'soil solid mass' as shown in Figure 2a and b. In this process, numerous intrapores will be produced, vast majority of them will be very small (e.g. a submicron to few microns in diameter) and therefore to quantify them, ultra-high resolution imaging devices is required. In this study, the resolution of the images was 30 μm, thus, it was not possible to get information about the pores below this size. A shift in pore size distribution towards more interpores and intrapores in compacted soils would force anaerobic conditions in soil, which affect microbial community structure and activity as well as biogeochemical processes (e.g. increase of $N_2O$ emissions) (Keller et al., 2013).

*4.2 Effect of soil moisture content on soil compaction*

The effect of soil compaction coupled with different soil moisture contents was evaluated in this study. Regardless of the effect of compaction, increasing soil moisture increased interpores volume and surface area while decreasing intrapores (Fig. 4). When focusing on the effect of soil moisture on soil compaction intensity, it was interesting to observe that soil compaction at water content of 9.8% (w/w) resulted in a greater reduction of interpores volume compared to 18.3% (w/w) soil water content. This was contrary to the hypothesis that higher soil moisture results in higher deformation of aggregates. Heterogeneity of soil aggregate packing into the cylinders could be a possible explanation of this finding. However, this possibility has been ruled out as the experiment used 2-5 mm sieved aggregates and initial weight was same for all replicates within each treatment. Hence, the hypothesis was revised such that addition of water caused a considerable increase in soil strength and stability and such behaviour was reported by Greacen (1960). When aggregates were dry (W1), they were more brittle and weak as suggested by Dexter (1988) earlier, thus more compressible compared to elevated moisture level (W2) for the given level of compaction (BD1). This additional shear strength of soil is explained by the force of surface tension between the soil particles when it is slightly moist. However, the application of higher compaction (BD2) could overcome the shear strength and thus lead to more compaction. The uni-axial load tests revealed the load applied to the samples with low moisture content was almost twice the load required to achieve the same level of compaction (BD1) at the higher moisture content (Table 1). A much higher load (530 kPa) was needed to achieve W2BD2 samples. However, it must be noted that multiple impacts during compaction in the experiment could additionally damage the structure of aggregates and reach the studied bulk densities earlier compared to the uni-axial test. The multiple impacts applied would have damaged more the dry samples compared to the moist ones (Dexter, 1988).

*4.3 Effect of compaction on soil interpore size distribution*

When strong compaction was applied to soil aggregates with elevated water content (W2), a substantial reduction of the proportion of interpore volume occurred with a corresponding rise in intrapore volume proportion (Fig. 4 a, b); and changes in the surface areas of pores followed a similar trend, but to a smaller extent. Furthermore, it is for the first time, using the X-ray tomography and 3D image analysis, that the real change in the interpore volume distribution in compacted soils was quantified. The number of pores was increased between 3 to 14 times by compaction, while the volume of pores drastically decreased by 5 to 20 times in compacted soils (Fig. 5). These changes, along with the increase in intrapores, will have implications in gas and water diffusion in soils as demonstrated by LBM simulations. Furthermore, such changes are likely to affect soil biology, as mainly small pores (0.001 $mm^3$) and disconnected from each other are present in compacted soil. Hence, soil compaction could negatively affect fungi because they are mainly located at the surface of aggregates and pores >10 μm (Chenu et al., 2001), while bacteria will be in pores potentially isolated from nutrient, oxygen and water input reducing their activity.

*4.4 Effect of compaction on water flow*

The aim of the LBM modelling exercise was to compare the effect on flow under various levels of compaction, without actually performing tedious flow experiments in the lab with the small volume of samples. The LBM was able to predict the magnitude of changes in flow in response to change in bulk density (or porosity) and it enabled simulation of the flow along with the quantification based on the real pore geometry obtained from the X-ray CT scanner. The flow was reduced by 97-99% when bulk density was 1.6 g $cm^{-3}$. However, it is important to note that LBM do not consider any soil properties or processes and ignores capillarity and unsaturated hydraulic conductivity. Prediction from LBM replies on digitised solid structure and is affected by how precise the real structure is represented. For example, 30 μm images resolution was used in this study, which missed crucial capillaries below this size. Hence, LBM results provide insights into fluid flow and it is used widely for trend analysis and therefore, the predictions need to be verified with real observations when working with soil samples. The model predictions were in good agreement with measurements in a previous study with sand (Menon et al., 2011) probably due to the resolution of the image used (2-3μm) and poor fluid interactions with sand grains. However, further modelling efforts are necessary to confirm the impact of compaction on unsaturated flow in soils as previously shown by Aravena et al (2014). Overall, the drastic reduction of water flow does not only increase the risk of soil erosion but also could affect other biogeochemical processes. For example, Li et al. (2002) reported that with an increase in soil BD from 1.00 to 1.60 g $cm^{-3}$, total numbers of bacteria, fungi and actinomycetes (measured by plate-counting technique) declined by 26–39% within the same soil mass.

## 5. Conclusions

The aim of the study was to develop a mechanistic understanding of pore system characteristics in compacted aggregates using 3D imaging and modelling tools. The main findings include:

1. XMT and image processing tools helped to gain deeper understanding of pore system changes in compacted soils. In this study a pore size range > 90 μm was sufficient to follow induced changes in soil structure in aggregates.
2. As a result of compaction, interpore volume and surface area decreased with corresponding increase in intrapores volume and surface area.
3. Compaction led to significant changes in interpore pore size distribution. The number of interpores increased by 3 to 14 times whereas its volumes were reduced by 5-20 times in the treatments.
4. The LBM simulations predicted a steep decline in flow with increase in bulk density. In our studied soil a bulk density larger 1.6 g $cm^{-3}$ would almost stop water flow.

Future compaction studies may include to understand the effect of soil particle size distribution and different moisture contents. It will be useful to measure the load applied prior to the imaging. More importantly, focus must be to understand how changes in pore size distribution in compacted soil affect soil biogeochemical processes.

## Acknowledgements

We acknowledge funding support from the European Commission FP 7 Collaborative Project "Soil Transformations in European Catchments" (SoilTrEC) (Grant Agreement no. 244118) and White Rose Collaboration Fund (2013-14). The authors would like to thank Taru Lehtinen for her help during the fieldwork. The authors would also like to thank Dr Leslie Coulten for his help and support with the CT scan, and Structure Vision Ltd for providing LBM support. We also thank Ms. Mehrabi for carrying out additional load tests at the University of Leeds. The authors would like to thank two anonymous reviewers for their valuable suggestions to improve the manuscript.

## References

Amézketa, E., 1999. Soil aggregate stability: a review. J. Sustain. Agric. 14, 83–151.

Aravena, J.E., Berli, M., Ruiz, S., Suárez, F., Ghezzehei, T.A., Tyler, S.W., 2014. Quantifying coupled deformation and water flow in the rhizosphere using X-ray microtomography and numerical simulations. Plant Soil 376, 95–110.

Banwart, S., 2011. Save our soils. Nature 474, 151–152.

Blaud, A., Lerch, T.Z., Chevallier, T., Nunan, N., Chenu, C., Brauman, A., 2012. Dynamics of bacterial communities in relation to soil aggregate formation during the decomposition of $^{13}$C-labelled rice straw. Appl. Soil Ecol. 53, 1–9.

Bossuyt, H., Six, J., Hendrix, P.F., 2002. Aggregate-protected carbon in no-tillage and conventional tillage agroecosystems using carbon-14 labeled plant residue. Soil Sci. Soc. Am. J. 66, 1965–1973.

Berli, M., Carminati, A., Ghezzehei, T., & Or, D. 2008. Evolution of unsaturated hydraulic conductivity of aggregated soils due to compressive forces. Water Resour. Res. 44.

Bronick, C.J and Lal, R. 2005. Soil Structure and management: a review. Geoderma 124, 3-22.

Carminati, A., Kaestner, A., Hassanein, R., Ippisch, O., Vontobel, P., & Flühler, H. 2007. Infiltration through series of soil aggregates: Neutron radiography and modeling. Adv. Water. Res. 30, 1168–1178.

Chenu, C., Hassink, J., Bloem, J., 2001. Short-term changes in the spatial distribution of microorganisms in soil aggregates as affected by glucose addition. Biol. Fertil. Soils 34, 349–356.

COM (2006) European Commission (online: http://ec.europa.eu/environment /soil/three_en.htm).

Dexter, A.R., 1988. Advances in characterization of soil structure. Soil Tillage Res., Proceedings 11th Conference of ISTRO: Tillage and Traffic in Crop Production 11, 199–238.

EEA (2012) Soil Compaction map of EU: http://www.eea.europa.eu/data-and-maps/figures/soil-compaction-in-europe.

FAO (Food and Agricultural Organization) http://www.fao.org/ag/ca/doc/soil_compaction.pdf (accessed on 02.07.2014)

Greacen, E.L., 1960. Water Content and Soil Strength. J. Soil Sci. 11, 313–333.

Hartemink, A.E., 2008. Soils are back on the global agenda. Soil Use Manag. 24, 327–330.

Haynes, R., Swift, R., 1990. Stability of soil aggregates in relation to organic constituents and soil water content. J. Soil Sci. 41, 73-83.

Hillel, D., 1998. Environmental Soil Physics: Fundamentals, Applications, and Environmental Considerations, Academic Press Inc. ed. Academic Press, San Diego.

Holtz et al (2010) Geotechnical Eng Prentice Hall (2nd Edition) p 174

Horn, R., Smucker, A., 2005. Structure formation and its consequences for gas and water transport in unsaturated arable and forest soils. Soil Tillage Res. 82, 5–14.

Keller, T., Lamandé, M., Peth, S., Berli, M., Delenne, J.-Y., Baumgarten, W., Rabbel, W., Radjaï, F., Rajchenbach, J., Selvadurai, A.P.S., Or, D., 2013. An interdisciplinary approach towards improved understanding of soil deformation during compaction. Soil Till. Res. 128, 61-80.

Lair, G.J., Zehetner, F., Hrachowitz, M., Franz, N., Maringer, F.-J., Gerzabek, M.H., 2009. Dating of soil layers in a young floodplain using iron oxide crystallinity. Quatern. Geochronol. 4, 260-266.

Li, C.H., Ma, B.L., Zhang, T.Q. 2002 Soil bulk density effects on soil microbial populations and enzyme activities during the growth of maize (*Zea mays* L.) planted in large pots under field exposure, Canadian J Soil Sci 82, 147-154.

Menon, M., Yuan, Q., Jia, X., Dougill, A.J., Hoon, S.R., Thomas, A.D., Williams, R.A., 2011. Assessment of physical and hydrological properties of biological soil crusts using X-ray microtomography and modeling. J. Hydrol. 397, 47–54.

Mooney, S.J., Pridmore, T.P., Helliwell, J., Bennett, M.J., 2012. Developing X-ray Computed Tomography to non-invasively image 3-D root systems architecture in soil. Plant Soil 352, 1–22.

Murphy, C.P., 1986. *Thin Section Preparation of Soils and Sediments*. A B Academic Publishers, Berkhamsted, UK.

R Development Core Team, 2013. R: a language and environment for statistical computing.

Sexstone, A.J., Revsbech, N.P., Bailey, T.B., Tiedje, J.M., 1985. Direct measurement of oxygen profiles and denitrification rates in soil aggregates. Soil Sci. Soc. Am. J. 49, 645–651.

Shein, E.V.2005. Course of Soil Physics (in Russian). Moscow State Univ. Publ., Moscow.

Six, J., Bossuyt, H., Degryze, S., Denef, K., 2004. A history of research on the link between (micro)aggregates, soil biota, and soil organic matter dynamics. Soil Till. Res. 79, 7–31.

Stamati F., N.P. Nikolaidis, S.A. Banwart and W.E. Blum, 2013. A Coupled Carbon, Aggregation, and Structure Turnover (CAST) Model for topsoils, GeoDerma, 211, 51-64

Tisdall, J.M., Oades, J.M., 1982. Organic matter and water-stable aggregates in soils. Eur. J. Soil Sci. 33, 141–163.

## Figure captions

**Fig. 1.** A 2D illustration of image processing steps followed in the study to differentiate interpores and intrapores. The above example is from a replicate before compaction.

**Fig. 2.** 3D view of soil aggregates before and after compaction. The images show the top 1 cm of a replicate from a sample with gravimetric water content 18.3% and bulk density before and after compaction before and after compaction 0.91 and 1.12 g cm$^{-3}$, respectively (W2BD2). Images on the left (a, c and e) show the solid phase (gold), interpores (red) and intrapores (yellow) before compaction, while the images on the right (b, d, and f) after compaction.

**Fig. 3.** Effect of soil compaction on total pores volume (a) and surface area (b) on soil aggregates with varying levels of soil moisture and compaction. Treatments key: W1 refers to moisture content of 9.3% and W2 represents 18.3 % (w/w); BD1 and BD2 refers to a bulk density increment of 0.28 and 0.71 g cm$^{-3}$, respectively (see Table 1). Means values ± standard deviation ($n$ = 6) are shown.

**Fig. 4.** Effect of soil compaction on interpores (a, c) and intrapores (b, d) volumes (a, b) and surface area (c, d) from soil aggregates with varying levels of soil moisture and compaction. The pores volume and surface area are expressed as proportion (%) of the total pores (interpores + intrapores) volume and surface area, respectively. Treatments key: W1 refers to moisture content of 9.3% and W2 represents 18.3 % (w/w); BD1 and BD2 refers to a bulk density increment of 0.28 and 0.71 g cm$^{-3}$, respectively (see Table 1). Means values ± standard deviation ($n$ = 6) are shown.

**Fig. 5.** Distribution of interpores volume (mm$^3$) and their number before (gray) and after soil compaction (black) in various treatments (a, b and c) applied. Please note that data from single replicate is shown. Treatment key: W1 refers to moisture content of 9.3% and W2 represents 18.3 % (w/w); BD1 and BD2 refers to a bulk density increment of 0.28 and 0.71 g cm$^{-3}$, respectively (see Table 1). NB: For better visualization, we have used a different scale for X-axis for b.

**Fig. 6.** Results from simulations using LBM; a) 2D cross sectional view of velocity distributions taken from a replicate with gravimetric water content 18.3% and with an increment in bulk density of 0.71 g $cm^{-3}$ (W2BD2, see Table 1 for details). Warm colours indicate higher values of real velocity and the soil appears in white; b) Relationship between the real velocity obtained by LBM simulations and bulk density (g $cm^{-3}$) of the samples with gravimetric water content of 18.3% with changes in bulk density (mean and standard deviations are shown; $n$ = 3, except at bulk density 0.92 $n$ = 6).

**Table 1.** Summary of treatments of the samples including gravimetric water content, initial and final bulk density (before and after soil compaction) and net change in bulk density.

| Treatment Combinations | Gravimetric water content (%) | Initial Bulk Density (g $cm^{-3}$) | Final Bulk density (g $cm^{-3}$) | Net change in bulk density (g $cm^{-3}$) | Equivalent Load (kPa) |
|---|---|---|---|---|---|
| W1 BD1 | 9.3 | 0.84 | 1.12 | 0.28 | 185 |
| W2 BD1 | 18.3 | 0.92 | 1.20 | 0.28 | 116 |
| W2 BD2 | 18.3 | 0.92 | 1.62 | 0.71 | 530 |

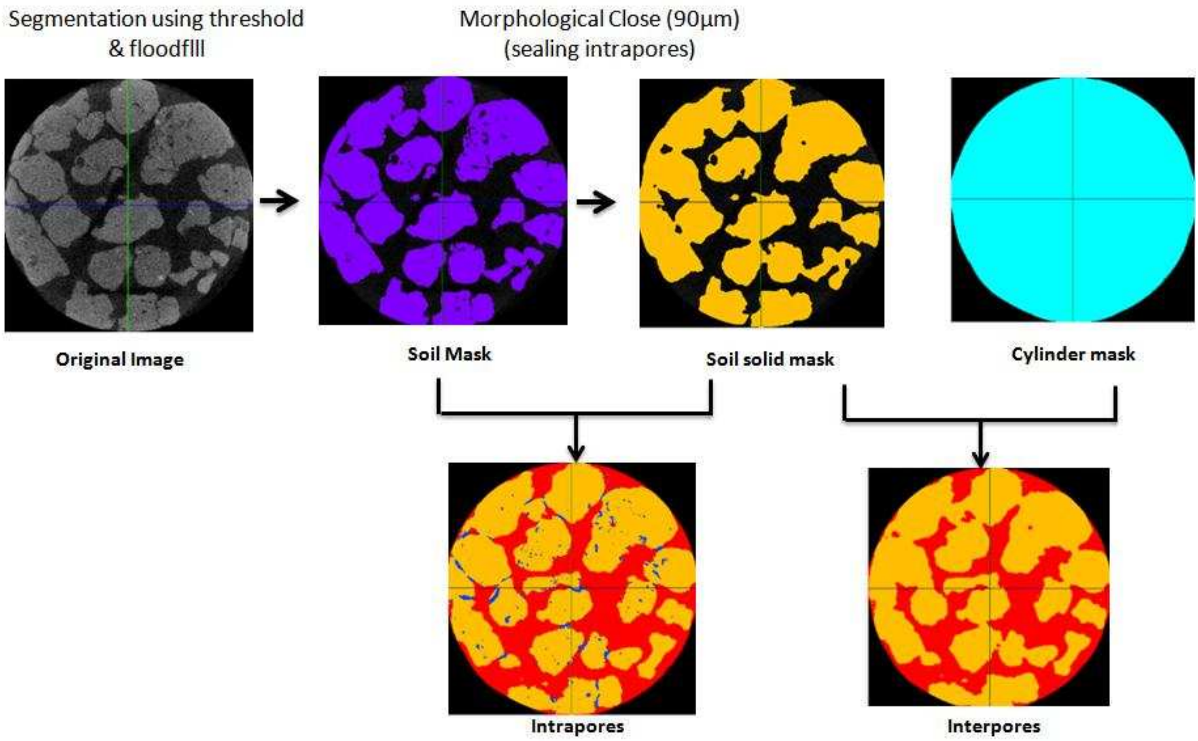


Fig. 1

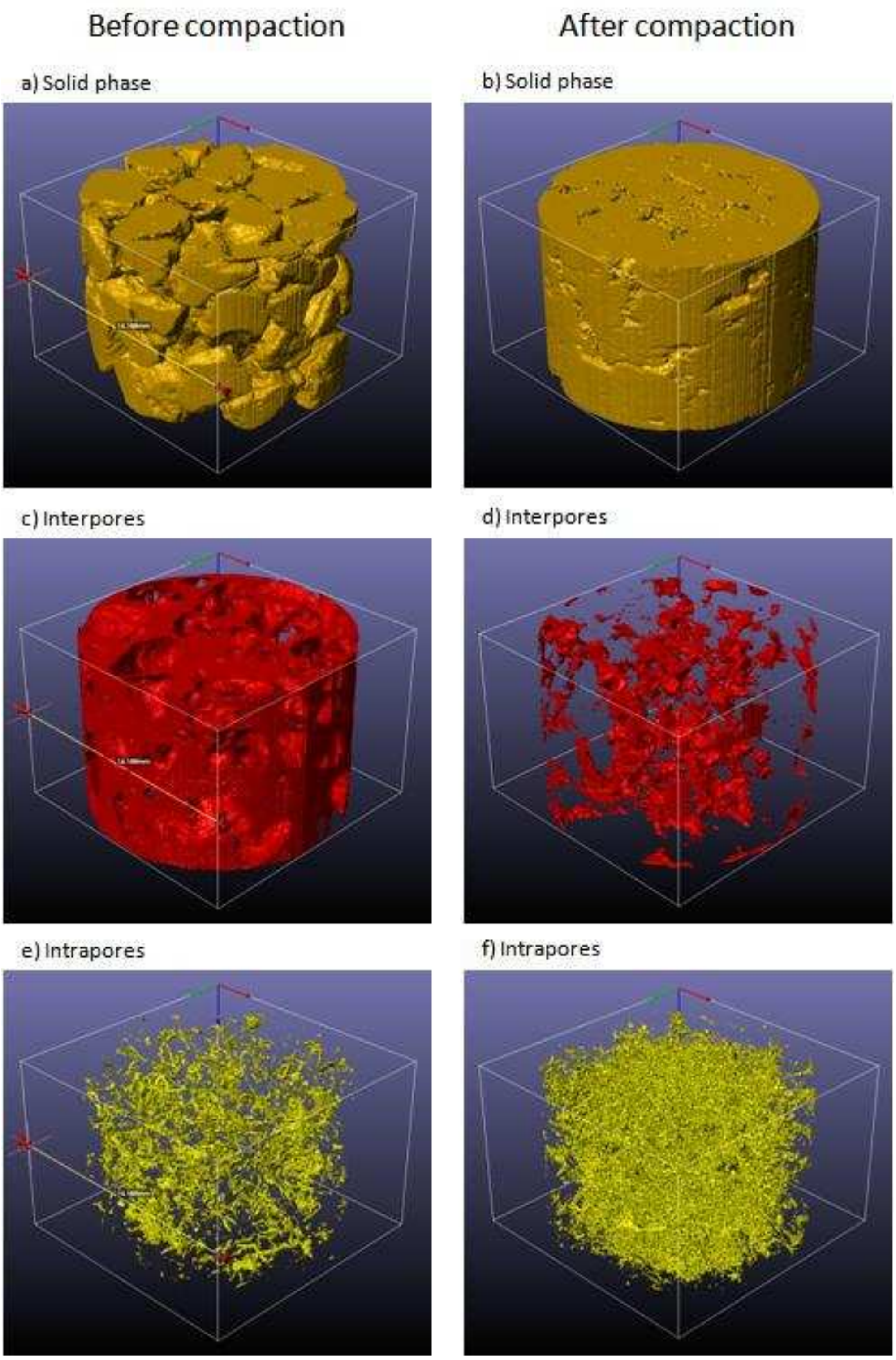
Before compaction
After compaction
a) Solid phase
b) Solid phase
c) Interpores
d) Interpores
e) Intrapores
f) Intrapores

Fig.2

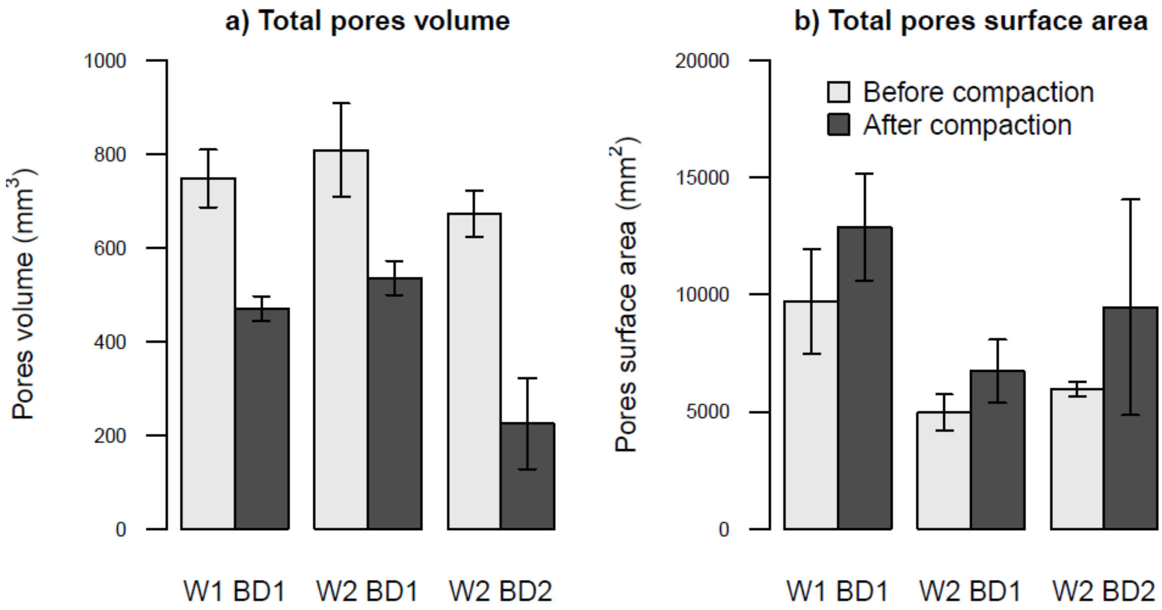

a) Total pores volume
Pores volume (mm3)
0
200
400
600
800
1000
W1 BD1
W2 BD1
W2 BD2
b) Total pores surface area
Pores surface area (mm2)
0
5000
10000
15000
20000
Before compaction
After compaction


Fig.3

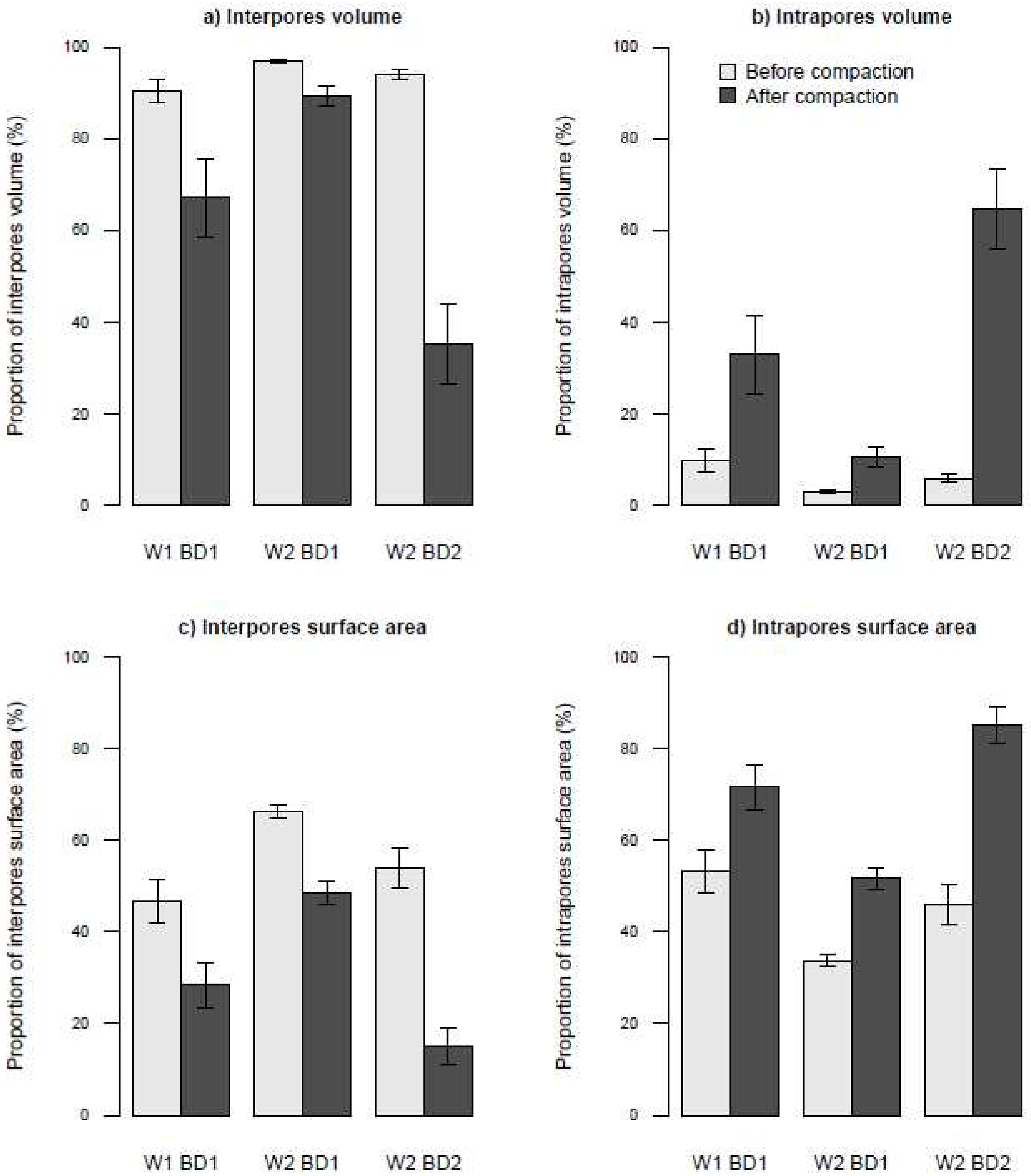
a) Interpores volume
b) Intrapores volume
Before compaction
After compaction
Proportion of interpores volume (%)
Proportion of intrapores volume (%)
W1 BD1
W2 BD1
W2 BD2
c) Interpores surface area
d) Intrapores surface area
Proportion of interpores surface area (%)
Proportion of intrapores surface area (%)

Fig.4

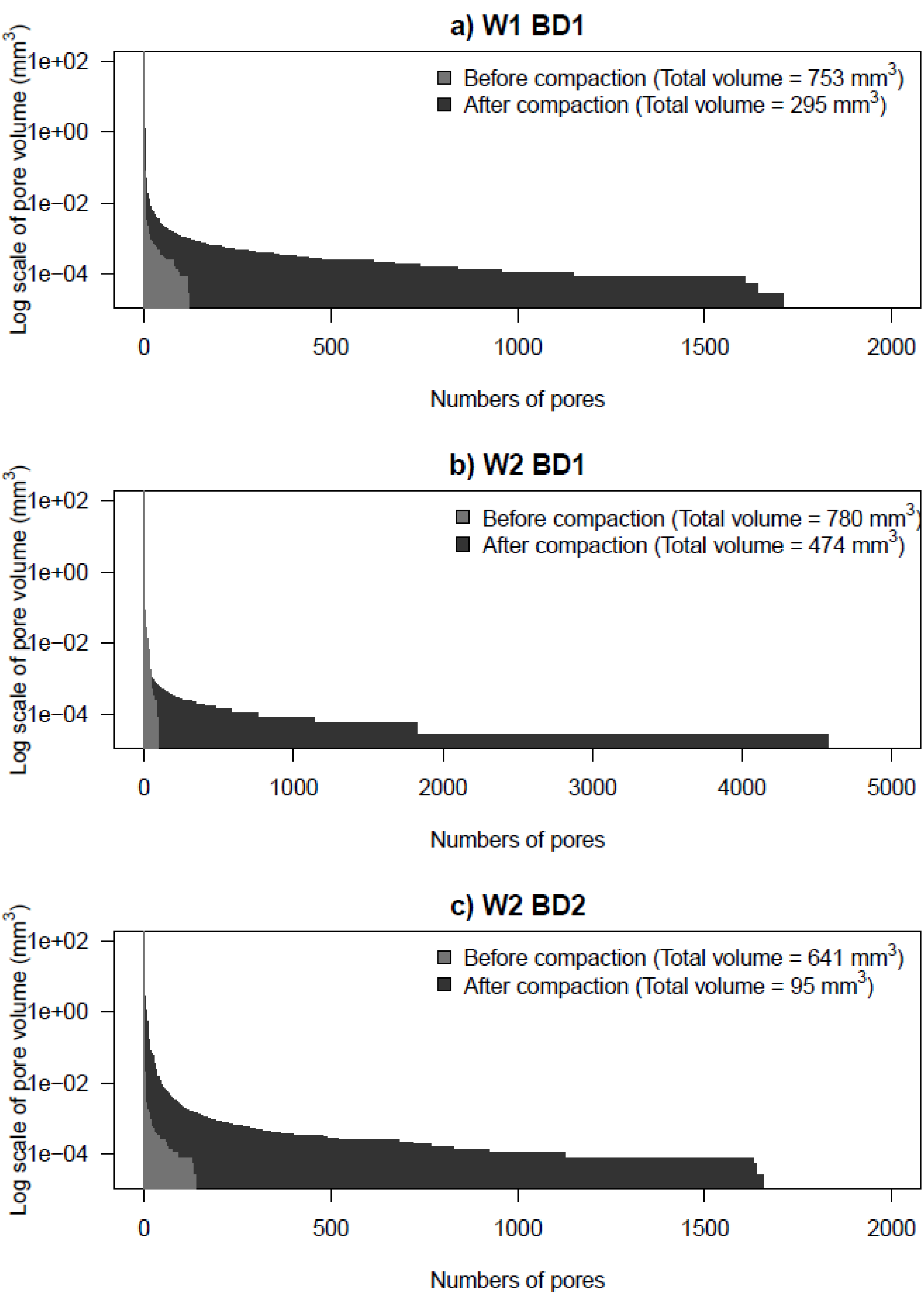
a) W1 BD1
Before compaction (Total volume = 753 mm3)
After compaction (Total volume = 295 mm3)
Log scale of pore volume (mm3)
1e+02
1e+00
1e−02
1e−04
0
500
1000
1500
2000
Numbers of pores
b) W2 BD1
Before compaction (Total volume = 780 mm3)
After compaction (Total volume = 474 mm3)
Log scale of pore volume (mm3)
1e+02
1e+00
1e−02
1e−04
0
1000
2000
3000
4000
5000
Numbers of pores
c) W2 BD2
Before compaction (Total volume = 641 mm3)
After compaction (Total volume = 95 mm3)
Log scale of pore volume (mm3)
1e+02
1e+00
1e−02
1e−04
0
500
1000
1500
2000
Numbers of pores

Fig.5

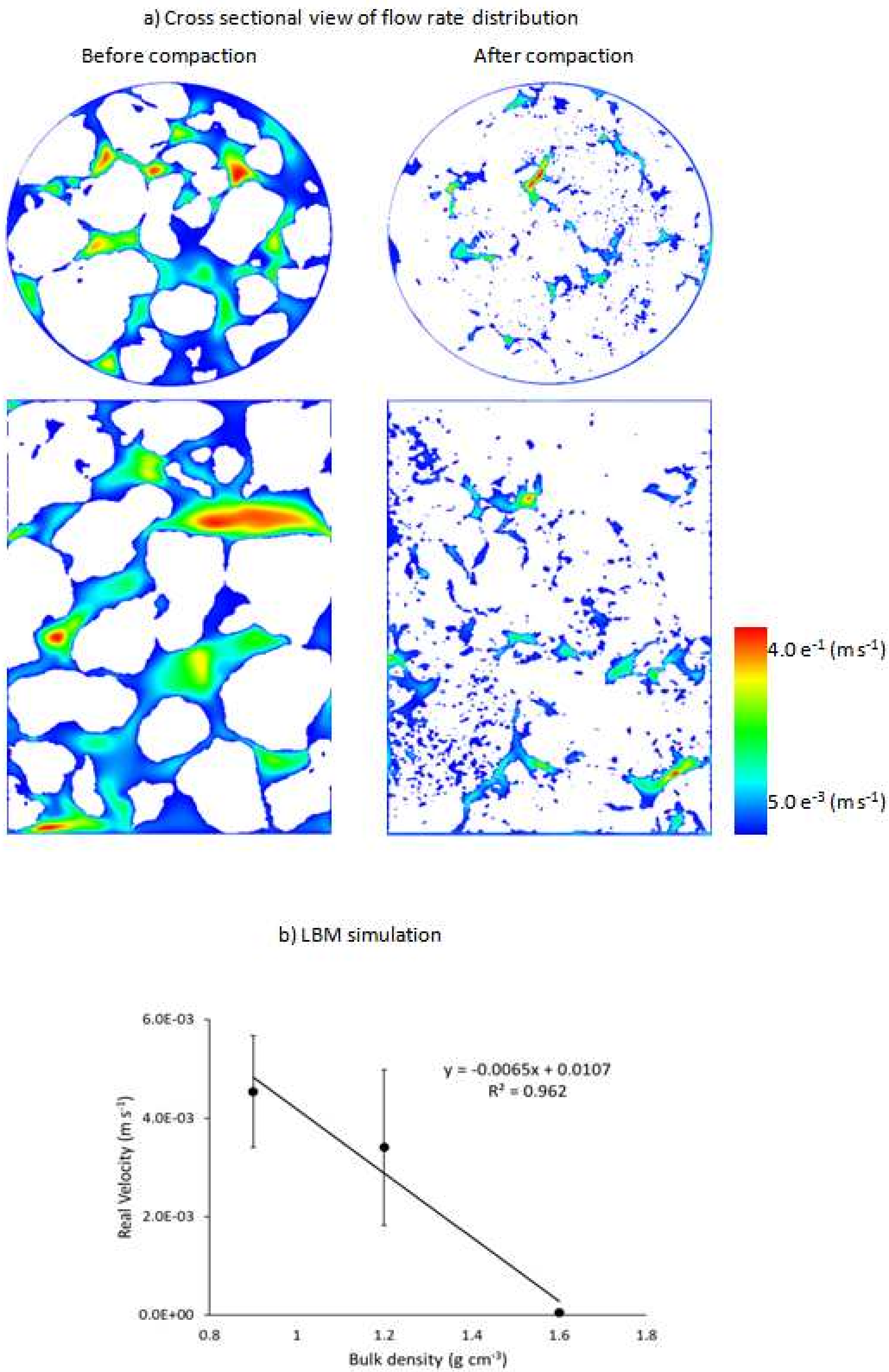
a) Cross sectional view of flow rate distribution
Before compaction
After compaction
4.0 e-1 (m s-1)
5.0 e-3 (m s-1)
b) LBM simulation
y = -0.0065x + 0.0107
R² = 0.962
Real Velocity (m s-1)
6.0E-03
4.0E-03
2.0E-03
0.0E+00
0.8
1
1.2
1.4
1.6
1.8
Bulk density (g cm-3)

Fig.6